Inorganic Chemistry

Article

pubs.acs.org/IC

Chemical Pressure and Rare-Earth Orbital Contributions in Mixed Rare-Earth Silicides $La_{5-x}Y_xSi_4$ ($0 \leq x \leq 5$)

Hui Wang, Fei Wang, Karah Jones, and Gordon J. Miller*

Department of Chemistry and Ames Laboratory, U.S. Department of Energy, Iowa State University, Ames, Iowa 50011, United States

Supporting Information

ABSTRACT: A crystallographic study and theoretical analysis of the structural and La/Y site preferences in the $La_{5-x}Y_xSi_4$ ($0 \leq x \leq 5$) series prepared by high-temperature methods is presented. At room temperature, La-rich $La_{5-x}Y_xSi_4$ phases with $x \leq 3.0$ exhibit the tetragonal Zr_5Si_4-type structure (space group $P4_12_12$, $Z = 4$, Pearson symbol $tP36$), which contains only Si−Si dimers. On the other hand, Y-rich phases with $x = 4.0$ and 4.5 adopt the orthorhombic Gd_5Si_4-type structure (space group $Pnma$, $Z = 4$, Pearson symbol $oP36$), also with Si−Si dimers, whereas Y_5Si_4 forms the monoclinic $Gd_5Si_2Ge_2$ structure (space group $P2_1/c$, $Z = 4$, Pearson symbol $mP36$), which exhibits 50% "broken" Si−Si dimers. Local and long-range structural relationships among the tetragonal, orthorhombic, and monoclinic structures are discussed. Refinements from single crystal X-ray diffraction studies of the three independent sites for La or Y atoms in the asymmetric unit reveal partial mixing of these elements, with clearly different preferences for these two elements. First-principles electronic structure calculations, used to investigate the La/Y site preferences and structural trends in the $La_{5-x}Y_xSi_4$ series, indicate that long- and short-range structural features are controlled largely by atomic sizes. La 5d and Y 4d orbitals, however, generate distinct, yet subtle effects on the electronic density of states curves, and influence characteristics of Si−Si bonding in these phases.

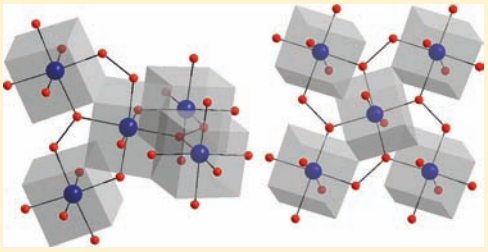

INTRODUCTION

The RE_5Si_4 and RE_5Ge_4 compounds (RE = rare earth metal) were first discovered by Smith et al.,[1,2] who later reported that all RE_5Ge_4 compounds (RE = La−Nd, Sm, Gd−Tm, Lu, and Y) crystallized in the orthorhombic Sm_5Ge_4-type structure,[3] whereas the RE_5Si_4 compounds crystallized in either the tetragonal Zr_5Si_4-type structure for phases with RE = La−Nd or the orthorhombic Gd_5Si_4-type structure for those with RE = Sm, Gd−Er, and Y.[3] After approximately 30 years of dormancy, these RE_5T_4 compounds and their pseudobinary, ternary, and other multicomponent analogues have become a goldmine for investigations in materials science, condensed matter physics, and solid state chemistry. Besides providing numerous opportunities to uncover fundamental structure−property relationships, these compounds have also produced practical materials, based on the discovery of a giant magnetocaloric effect (MCE) in $Gd_5Si_2Ge_2$ in 1997, along with other extraordinary magnetic properties, such as colossal magnetostriction and giant magnetoresistance.[4−13]

Among investigations on RE_5T_4 systems (T = element from groups 13−15), most have focused on the pseudobinary mixed silicide-germanide $RE_5(Si_xGe_{1-x})_4$ systems, many of which adopt at least three different crystal structures as the Si:Ge ratio varies.[14] These studies have uncovered some intriguing relationships among chemical compositions, crystal structures, and properties, but all reveal the importance of the purity of the elements used to prepare these compounds. For example, in 2004, Pecharsky et al. found that Y_5Si_4 crystallizes in the monoclinic $Gd_5Si_2Ge_2$-type structure,[15] rather than the orthorhombic Gd_5Si_4-type. In $RE_5(Si_xGe_{1-x})_4$ systems, interstitial impurities, for example, carbon atoms, typically stabilize the orthorhombic Sm_5Ge_4-type or Gd_5Si_4-type crystal structures in the range of concentrations where the monoclinic $Gd_5Si_2Ge_2$-type structure was found to be stable when high purity Gd was used to prepare the compounds.[15−17] In addition, these light atom impurities, such as H, C, N, and O, can even eliminate any magneto-structural transformations.

On the other hand, much fewer pseudobinary $(RE_xRE'_{1-x})_5Si_4$ and $(RE_xRE'_{1-x})_5Ge_4$ systems have been explored. In these mixed rare earth systems, a primary goal has been to examine the effect of chemical pressure exerted by different combinations of rare earth metals on magneto-responsive behavior, rather than any structural influences. Nonetheless, in the germanide system, $(La_xGd_{1-x})_5Ge_4$, both binary end members La_5Ge_4 and Gd_5Ge_4 adopt the orthorhombic Sm_5Ge_4-type whereas an intermediate composition, $La_2Gd_3Ge_4$ shows the monoclinic $Gd_5Si_2Ge_2$-type.[18] Throughout the entire series, the larger La atoms preferentially occupy atomic sites that have noticeably larger bond distances with Ge. In the $(Y_xGd_{1-x})_5Ge_4$ system, on the other hand, a new monoclinic $U_2Mo_3Si_4$-type structure occurs for certain Y-rich compositions.[19] Furthermore, analysis of site occupancies of the metal atom positions indicated that Y atoms prefer sites which show the shortest metal−metal contacts. Similar results have been obtained for $(Lu_xGd_{1-x})_5Ge_4$ and $(Sc_xGd_{1-x})_5Ge_4$.[20]

Received: August 23, 2011
Published: November 22, 2011

Among the silicides, reports on $Gd_xTb_{5-x}Si_4$, $Gd_xEr_{5-x}Si_4$, and $Gd_xY_{5-x}Si_4$ systems indicate that all crystallize in the orthorhombic Gd_5Si_4-type. For $(RE_xRE'_{1-x})_5Si_4$ cases with mixtures of early RE and late RE′ metals, for example, $Nd_xEr_{5-x}Si_4$, a structural transition occurs from the orthorhombic Gd_5Si_4-type to tetragonal Zr_5Si_4-type as the Nd content increases.[20] In $Pr_xGd_{5-x}Si_4$, however, a similar transformation can be predicted from the two end members, that is, orthorhombic Gd_5Si_4 and tetragonal Pr_5Si_4, but there are only reports of Gd-rich cases, $PrGd_4Si_4$, $Pr_{0.75}Gd_{4.25}Si_4$, and $Pr_{0.5}Gd_{4.5}Si_4$, which adopt the orthorhombic structure.[21] Since the rare earth metals in these silicides have unpaired 4f electrons, there can be magneto-structural correlations influencing these transitions.

Therefore, in this contribution we focus on $(RE_xRE'_{1-x})_5Si_4$ with a mixture of "nonmagnetic" rare earth metals, that is, $La_xY_{5-x}Si_4$, to investigate this structural transition in the absence of possible magnetic ordering mechanisms. Recently, a related study emerged for $Zr_xHf_{5-x}Ge_4$, for which a structural transition from orthorhombic to tetragonal occurs as the Zr content increases,[22] but this case involves tetravalent metals. Also, the structures of specific examples of related compounds $RE_2RE'_3Si_4$ (RE = La, Ce; RE′ = Y, Lu) are reported, namely, $La_{1.72}Y_{3.28}Si_4$, $La_{1.72}Lu_{3.28}Si_4$, $Ce_{1.71}Y_{3.29}Si_4$, and $Ce_{1.82}Lu_{3.18}Si_4$.[23] Although the structures of La_5Si_4 and Y_5Si_4 have been reported,[15,23−25] our examination of the pseudobinary $(La_{5-x}Y_x)Si_4$ system not only investigates relationships between the tetragonal Zr_5Si_4-type and orthorhombic Gd_5Si_4-type structures, but also probes the distribution of differently sized, nonmagnetic rare earth metals in these structures. In this study, replacing La by the smaller Y atoms acts as a "chemical pressure," which induces a structural change. However, this mechanical argument ignores possible effects on electronic structure. Herein, we report their preparation, crystal structures, and analysis of electronic structures for the series $(La_{5-x}Y_x)Si_4$.

EXPERIMENTAL SECTION

Preparation. Seven samples of loaded compositions $La_{5-x}Y_xSi_4$, where x = 0, 1.0, 2.0, 3.0, 4.0, 4.5, and 5.0, were prepared by arc-melting about 1.0 g mixtures of the constituent elements under an argon atmosphere on a water-cooled copper hearth using high purity yttrium and lanthanum obtained from the Materials Preparation Center of Ames Laboratory (The major metal atom impurity in La and Y is Ce, at a level less than 1 ppm by mass; the major nonmetal impurity is F, which is analyzed at a level less than 5 ppm by mass). Silicon (99.9999 wt %, Alfa Aesar) was used as purchased. Each arc-melted pellet was turned over and remelted six times to ensure homogeneity; subsequent weight losses during melting were less than about 0.1 wt %. After reaction, every product yielding a tetragonal phase was broken into halves: one-half was submitted directly for characterization; the other half was sealed in a tantalum tube in an argon atmosphere, then jacketed in evacuated silica tubes, and subsequently annealed at 1000 °C for 24 h. After annealing, the tubes were quenched in cold water. All products remained stable toward decomposition after storage in air for several months.

Phase Analysis by Powder X-ray Diffraction. Powder X-ray diffraction patterns for as-cast and annealed samples were collected using a Huber 670 Guinier camera with monochromated CuK_α radiation (λ = 1.54187 Å) at room temperature. The step size was set at 0.005°, and the exposure time was 1−2 h. Data acquisition was controlled via the in situ program. To investigate the purity and homogeneity of all samples, all diffraction patterns were analyzed by Le-Bail refinement using the LHPM Rietica software.[26] Only the scale factors, peak profiles, backgrounds, and lattice parameters of the $La_{5-x}Y_xSi_4$ phases in each sample were refined, using Si powder (NIST; a = 5.430940 ± 0.000035 Å) as a calibration standard. All values were in good agreement with the results from single crystal X-ray diffraction.

Structural Analysis by Single Crystal X-ray Diffraction. Several single crystals from the as-cast samples were glued on the tips of glass fibers. Room temperature intensity data were collected on a Bruker Smart Apex CCD diffractometer with Mo K_α radiation (λ = 0.71073 Å) and a detector-to-crystal distance of 5.990 cm. Data were collected over a full sphere of reciprocal space by taking three sets of 606 frames with 0.3° scans in ω and with an exposure time of 10 s per frame. The range of 2θ extended from 4° to 57°. The data were acquired using SMART software.[27] Data integration and cell refinement was carried out with the SAINT+ program.[28] Empirical absorption correction was done with the SADABS software.[29] Structure solutions and refinements were performed with the SHELXTL[30] package of crystallographic programs. Further details of the crystal structure investigations are available from the Fachinformationszentrum Karlsruhe, 76344 Eggenstein-Leopoldshafen, Germany, on quoting the depository number CSD-423412($La_{3.97}Y_{1.02}Si_4$), CSD-423413($La_{1.85}Y_{3.15}Si_4$), CSD-423414($La_{0.75}Y_{4.24}Si_4$), and CSD-423415-($La_{0.48}Y_{4.52}Si_4$), the name of the authors, and citation of the paper.

Electronic Structure Calculations. To explore site preferences for La and Y atoms and volume effects for $La_{5-x}Y_xSi_4$ structures, first-principles electronic structure calculations were performed with the Vienna ab initio simulation package (VASP)[31−34] and the Stuttgart tight-binding, linear-muffin-tin orbital program with the atomic spheres approximation (TB-LMTO-ASA).[35] Structural models of La_5Si_4, "La_4YSi_4", "LaY_4Si_4", and Y_5Si_4 used for these computations were constructed according to the diffraction results.

All VASP calculations were performed using projector augmented-wave (PAW) pseudopotentials.[36] A 7 × 7 × 7 Monkhorst-Pack k-points grid was used to sample the first Brillouin zone for reciprocal space integration.[37] The energy cutoff of the plane wave basis was 245 eV. With these settings, the total energies converged to less than 1 meV per unit cell.

TB-LMTO-ASA calculations were carried out to examine the orbital interactions via analysis of electronic densities of states (DOS) and crystal orbital Hamilton population (COHP) curves.[38] For these calculations, the von Barth−Hedin local density approximation[39] was employed for the treatment of exchange and correlation energy. All relativistic effects except spin−orbit coupling were taken into account using a scalar relativistic approximation.[40] The basis set included La 6s, 6p, and 5d orbitals, Y 5s, 5p, and 4d orbitals, and Si 3s, 3p, and 3d orbitals. The La 6p, Y 5p, and Si 3d orbitals were treated by the Löwdin downfolding technique.[41] The Wigner−Seitz radii of the atomic spheres were 1.858−2.074 Å for La and Y, and 1.485−1.503 Å for Si, values which filled the unit cell with about 8.37% overlap without introducing any empty spheres. A total of 256 (8 × 4 × 8) k-points in the irreducible wedge of the orthorhombic first Brillouin zone were used for integration.

RESULTS AND DISCUSSION

Phase and Structural Analysis of $La_{5-x}Y_xSi_4$. The powder X-ray diffraction patterns of all as-cast samples of $La_{5-x}Y_xSi_4$ (x = 0, 1.0, 2.0, 3.0, 4.0, 4.5, 5.0) have been collected for phase identification and to assess phase purity. In these samples, we observe three distinct phases: (i) for $x \leq 3.0$, the tetragonal Zr_5Si_4-type structure (space group $P4_12_12$, Z = 4) occurs as the main phase; (ii) for x = 4.0 and 4.5, the orthorhombic Gd_5Si_4-type structure (space group $Pnma$, Z = 4) occurs with no secondary phases observable; and (iii) for x = 5.0, the monoclinic structure (space group $P2_1/c$, Z = 4) occurs. In $La_{5-x}Y_xSi_4$ samples loaded with $0 \leq x \leq 3.0$, a secondary phase could be detected, so these samples were annealed at 1000 °C for 24 h. For La_5Si_4 and La_4YSi_4 samples, samples before and after annealing showed two phases by powder diffraction; the minority phase can be indexed as FeB-type

dx.doi.org/10.1021/ic201840q | Inorg. Chem. 2011, 50, 12714−12723

$La_{1-x}Y_xSi$.[25,42] For $La_2Y_3Si_4$ and $La_3Y_2Si_4$ samples, the impurity phase is much less distinctive, and their diffraction peaks are very broad and cannot be unambiguously indexed. In the following, therefore, we describe results derived from just the majority phases extracted from as-cast samples. The refined lattice parameters obtained from the majority phases from $La_{5-x}Y_xSi_4$ by powder X-ray diffraction are listed in Table 1.

Table 1. Crystallographic Data for $La_{5-x}Y_xSi_4$ As Obtained by Powder X-ray Diffraction

x in $La_{5-x}Y_xSi_4$	a (Å)	b (Å)	c (Å)	V (Å^3)
0	8.051(1)	8.051(1)	15.442(1)	1001.0(1)
1.0	7.977(2)	7.977(2)	15.058(1)	958.1(2)
2.0	7.902(1)	7.902(1)	14.566(1)	909.7(2)
3.0	7.808(1)	7.808(1)	14.380(1)	876.6(1)
4.0	7.447(1)	14.694(1)	7.756(1)	848.7(1)
4.5	7.421(1)	14.635(1)	7.723(1)	838.8(2)
5	14.603(1)	7.659(1)	7.462(1)	833.2(2)

The unit cell volumes decrease linearly with increasing Y content, in agreement with the smaller size of Y as compared to La.[43] There is also very good agreement with Zen's law,[44] which is a linear relationship between unit cell volume and chemical composition, along the entire range.

Single crystal diffraction was used to refine atomic parameters in many of these phases. The crystallographic data, atomic positions, site occupancies, and isotropic displacement parameters obtained by single crystal X-ray diffraction from samples extracted from each as-cast product are listed in Tables 2 and 3. The tetragonal Zr_5Si_4-type and orthorhombic Gd_5Si_4-type structures both have three crystallographically independent sites for La or Y atoms, all of which show similar chemical environments, which we have labeled accordingly as "M1", "M2", and "M3" to correspond with the numbering scheme in Table 3 (M = La, La/Y, or Y). The monoclinic structure of Y_5Si_4 has five independent metal atom sites, but their environments closely resemble those from the orthorhombic structure, so we have labeled the Y atoms according to their coordination resemblances, which are determined by constructing convex polyhedra around each site. The M1 sites have coordination number (CN) 18 with 7 Si and 11 rare earth atoms in the coordination shell. The M2 sites have a lower CN 16 with 6 Si and 10 rare earth atoms. The M3 positions have the even lower CN 14 with 6 Si and 8 rare-earth neighbors. In accordance with these coordination numbers, the volumes associated with each "M" site, as evaluated by the program DIDO95,[45] show that the M1 and M2 site volumes are, respectively, 17−20% and 3−6% larger than the M3 site volume. As Table 3 also summarizes, each structure shows various inequivalent crystallographic sites for the Si atoms, although they all show CN 9 created by tricapped trigonal prisms formed by 8 La/Y atoms and 1 capping Si atom. Finally, the refined compositions, which are listed in Table 2 and calculated from site occupancies presented in Table 3, are in excellent agreement with the loaded compositions

Although the three crystal structure types exhibit similar atomic coordination, the structures are distinct in two different ways: (1) as networks of M3-centered polyhedra; and (2) structures and connectivities associated with the silicide groups. Figure 1 illustrates the difference between the tetragonal and the orthorhombic/monoclinic structures from the perspective of the network of M3-centered polyhedra. All three structure types have the same building block, which is a $(M3)M_8$ cube (M3-centered cube of rare-earth atoms made of M1 and M2 atoms) with each face capped by Si atoms. Moreover, each of these $(M3)M_8$ cubes is linked to four adjacent cubes by sharing edges, but they differ in the orientation of these shared edges. In the tetragonal Zr_5Si_4-type structure, the $(M3)M_8$ cubes form a three-dimensional network with 4_1 screw axes. The network is created by each $(M3)M_8$ cube sharing pairs of orthogonal cubic edges with its four neighboring $(M3)M_8$ cubes. In orthorhombic Gd_5Si_4-type and monoclinic $Gd_5Si_2Ge_2$-type structures, on the other hand, the $(M3)M_8$ cubes are condensed via four parallel edges to create planar slabs extending in the ***a***- and ***c***-directions. These layers stack along the crystallographic ***b***-axis.

From the perspective of the silicide substructure, the three structure types also differ. In the tetragonal and orthorhombic structure types, which occur for $La_{5-x}Y_xSi_4$ ($x \leq 4.5$), all Si atoms form Si−Si dimers, with these distances ranging from 2.463(1) Å in La_5Si_4 to 2.589(2) Å in LaY_4Si_4. Within the series of tetragonal structures, $La_{5-x}Y_xSi_4$ ($x \leq 3.0$), all Si−Si dimers are crystallographically equivalent and show increasing distance with increasing Y content (from 2.463(1) Å in La_5Si_4 to 2.567(3) Å in $La_{1.85(7)}Y_{3.15}Si_4$), although the unit cell volume decreases. In the orthorhombic structures, $La_{5-x}Y_xSi_4$ (x = 4.0,

Table 2. Crystallographic Data for $La_{5-x}Y_xSi_4$ (x = 0, 1.0, 3.0, 4.0, 4.5, 5) As Obtained by Single Crystal X-ray Diffraction. [a]

loaded comp.	La_5Si_4	La_4YSi_4	$La_2Y_3Si_4$	LaY_4Si_4	$La_{0.5}Y_{4.5}Si_4$	Y_5Si_4
ref. comp.	La_5Si_4	$La_{3.97(4)}Y_{1.03}Si_4$	$La_{1.85(7)}Y_{3.15}Si_4$	$La_{0.75(2)}Y_{4.25}Si_4$	$La_{0.48(2)}Y_{4.52}Si_4$	Y_5Si_4
sp. gr.	$P4_12_12$	$P4_12_12$	$P4_12_12$	$Pnma$	$Pnma$	$P2_1/c$
struct. type	Zr_5Si_4	Zr_5Si_4	Zr_5Si_4	Gd_5Si_4	Gd_5Si_4	$Gd_5Si_2Ge_2$
a (Å)	8.059(2)	7.973(2)	7.808(1)	7.453(1)	7.426(1)	14.625(2)
b (Å)	8.059(2)	7.973(2)	7.808(1)	14.722(3)	14.647(3)	7.671(1)
c (Å)	15.450(5)	15.013(4)	14.396(3)	7.770(1)	7.734(1)	7.473(1)
β (deg)						93.343(3)
V (Å^3)	1003.4(5)	954.3(4)	877.6(2)	852.5(3)	841.2(2)	837.0(2)
ind. refl.	1220	1159	1058	1073	1037	2006
no. par.	43	45	45	48	47	82
R1, $I > 2\sigma(I)$	0.0374	0.0400	0.0408	0.0365	0.0532	0.0440
wR2, $I > 2\sigma(I)$	0.0612	0.0672	0.0628	0.0568	0.0830	0.0735
peak (e$^-$/Å^3)	1.390	1.421	1.357	1.625	1.876	1.376
hole (e$^-$/Å^3)	−1.458	−1.406	−1.211	−1.088	−1.501	−1.381

[a] Mo Kα radiation, 2θ range = 4−57°, T = 298 K, Z = 4.

dx.doi.org/10.1021/ic201840q | Inorg. Chem. 2011, 50, 12714−12723

Table 3. Atomic Coordinates (×10^4), Site Occupancies, And Isotropic Displacement Parameters (Å^2;×10^3) for $La_{5-x}Y_xSi_4$ (x = 0, 1.0, 3.0, 4.0, 4.5, 5)

atom	site	x	y	z	occupancy	U_{eq}
			--- La_5Si_4 ---			
La(1)	8*b*	1247(1)	4877(1)	4497(1)	1.0	14(1)
La(2)	8*b*	1265(1)	191(1)	3740(1)	1.0	12(1)
La(3)	4*a*	1916(1)	1916(1)	0	1.0	15(1)
Si(1)	8*b*	3306(5)	3020(4)	2980(2)	1.0	14(1)
Si(2)	8*b*	2894(5)	792(4)	1910(2)	1.0	14(1)
			--- La_4YSi_4 ---			
La(1)	8*b*	1314(1)	4888(1)	4538(1)	1.0	15(1)
La(2)/Y(2)	8*b*	1313(1)	161(1)	3747(1)	0.68(1)/0.32	14(1)
La(3)/Y(3)	4*a*	1881(1)	1881(1)	0	0.61(1)/0.39	16(1)
Si(1)	8*b*	3380(5)	2990(5)	3029(2)	1.0	19(1)
Si(2)	8*b*	2891(5)	741(5)	1902(2)	1.0	17(1)
			--- $La_2Y_3Si_4$ ---			
La(1)/Y(1)	8*b*	1424(1)	4914(1)	4593(1)	0.85(2)/0.15	13(1)
La(2)/Y(2)	8*b*	1399(1)	96(1)	3757(1)	0.06(1)/0.94	11(1)
La(3)/Y(3)	4*a*	1823(2)	1823(2)	0	0.05(1)/0.95	13(1)
Si(1)	8*b*	3481(5)	2955(4)	3103(2)	1.0	13(1)
Si(2)	8*b*	2906(4)	628(4)	1883(2)	1.0	13(1)
			--- LaY_4Si_4 ---			
La(1)/Y(1)	8*d*	215(1)	5966(1)	1792(1)	0.38(1)/0.62	13(1)
Y(2)	8*d*	3196(1)	1228(1)	1778(1)	1.0	12(1)
Y(3)	4*c*	1526(1)	2500	5121(1)	1.0	12(1)
Si(1)	8*d*	1492(3)	397(2)	4701(3)	1.0	15(1)
Si(2)	4*c*	243(4)	2500	1099(4)	1.0	13(1)
Si(3)	4*c*	2702(4)	2500	8745(4)	1.0	13(1)
			--- $La_{0.5}Y_{4.5}Si_4$ ---			
La(1)/Y(1)	8*d*	224(1)	5966(1)	1797(1)	0.24(1)/0.76	14(1)
Y(2)	8*d*	3195(2)	1227(1)	1782(1)	1.0	11(1)
Y(3)	4*c*	1516(2)	2500	5121(2)	1.0	11(1)
Si(1)	8*d*	1495(5)	0398(2)	4706(4)	1.0	14(1)
Si(2)	4*c*	245(7)	2500	1070(6)	1.0	15(1)
Si(3)	4*c*	2690(6)	2500	8746(6)	1.0	12(1)
			--- Y_5Si_4 ---			
Y(1a)	4*e*	5984(1)	3201(1)	4953(1)	1.0	12(1)
Y(1b)	4*e*	990(1)	6817(1)	4801(1)	1.0	12(1)
Y(2a)	4*e*	1218(1)	1781(1)	3274(1)	1.0	10(1)
Y(2b)	4*e*	3802(1)	1651(1)	3541(1)	1.0	11(1)
Y(3)	4*e*	2533(1)	5061(1)	1736(1)	1.0	11(1)
Si(1a)	4*e*	408(2)	4720(3)	1485(3)	1.0	13(1)
Si(1b)	4*e*	4575(2)	4656(3)	2032(3)	1.0	12(1)
Si(2)	4*e*	2481(2)	1084(3)	456(3)	1.0	14(1)
Si(3)	4*e*	7517(2)	3709(3)	2112(3)	1.0	12(1)

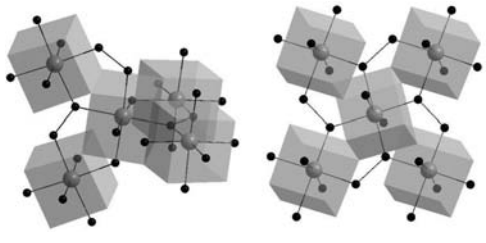

Figure 1. Two different ways the edges of the cubes of RE metals surround the M3 site (large gray spheres) are fused with adjacent units to form the (left) tetragonal and (right) orthorhombic structures. Small black spheres represent silicon atoms.

4.5), there are two structurally distinct Si−Si dimers: (i) Si2−Si3 units within the layers, shown in Figure 1; and (ii) Si1−Si1 dimers, which connect adjacent layers along the ***b***-axis. Please see Supporting Information for a complete illustration of the different structures. The Si−Si distances in these orthorhombic, Y-rich cases (2.555(3) and 2.549(3) Å) are similar to each other and resemble the Si−Si distance in tetragonal $La_{1.85(7)}Y_{3.15}Si_4$. Finally, monoclinic Y_5Si_4 shows three different types of silicide substructures, two of which are dimers as in the orthorhombic case. Here, the Si2−Si3 distance is 2.573(2) Å, but one set of Si1−Si1 dimers (Si1a−Si1a) connects adjacent layers at 2.494(6) Å. Another set of Si1−Si1 "dimers" (Si1b−Si1b) exhibit a nonbonded distance of 3.388(7) Å.[46]

Coloring Problem in $La_{5-x}Y_xSi_4$. The coloring problem, better known as the "four-color problem" in mathematics, describes the distribution of different elements over various independent sites in a structure when it is applied in chemistry.[47] Although electronic and geometric factors often dictate atomic distributions, the entropy contribution to the

dx.doi.org/10.1021/ic201840q | *Inorg. Chem.* 2011, 50, 12714−12723

Gibbs free energy always favors a statistical mixture.[48,49] However, in as-cast $La_{5-x}Y_xSi_4$ compounds, there are clear site preferences for Y and La atoms among the metal sites, an effect which implies a significant enthalpic contribution to the distribution. The variation in Y site occupancies for the M1, M2, and M3 sites in $La_{5-x}Y_xSi_4$ are illustrated in Figure 2. In the tetragonal structures, which are La-rich, the M1 site is strongly preferred for La, and shows no mixed occupancy until $La_2Y_3Si_4$. On the other hand, the other two metals sites (M2 and M3) show mixing of La and Y. From the coordination environments, La prefers to occupy the site with the greatest volume and largest coordination number. Now, for the Y-rich orthorhombic structures, La atoms exclusively, but partially, replace Y atoms in the M1 sites. As in the tetragonal structures, these M1 sites show the largest volumes and coordination numbers.

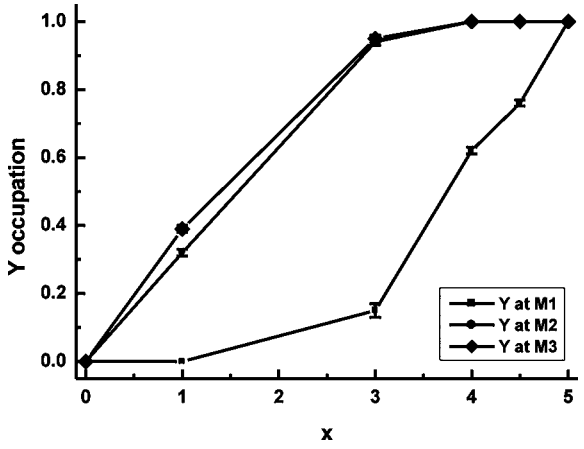

Figure 2. Occupancy of Y atoms in the M1, M2, and M3 sites of $La_{5-x}Y_xSi_4$ (x = 0, 1.0, 3.0, 4.0, 4.5, 5) as a function of Y content, taken from refinements of single crystal diffraction data at room temperature.

To investigate the distribution of Y and La atoms among the M1, M2, and M3 sites in $La_{5-x}Y_xSi_4$, we constructed different computational models for tetragonal "La_4YSi_4" and orthorhombic "LaY_4Si_4," according to the results obtained from the refinements of powder and single-crystal X-ray diffraction. Fragments of these models are illustrated in Figures 3 and 4. Of the three tetragonal models for "La_4YSi_4," models (**A**) and (**B**) involve breaking the equivalence of the M1 (8*b*) and M2 (8*b*) sites in space group $P4_12_12$ by placing 4 La and 4 Y atoms among each of these 8 positions in the unit cell. Model (**C**) has Y atoms at the M3 (4*a*) sites, which requires no adjustment of the space group. In Models (**B**) and (**C**), there are only La−Y near neighbor contacts; Model (**A**) includes Y−Y near neighbor contacts, too. Likewise, the distribution of La atoms in orthorhombic "LaY_4Si_4" breaks equivalences of sites in space group *Pnma* when La occupies the M1 or M2 sites, as seen in Models (**A1**), (**A2**), (**B1**), and (**B2**). Furthermore, (**A2**) removes the mirror plane contained by each layer. As for the tetragonal cases, these models differ in the types of metal−metal close contacts. Just model (**C**) has only La−Y near neighbor contacts; in the remaining models, there are La−La near neighbor contacts, but they occur with different distance values, which are included in Figure 4.

To compare these coloring schemes, first principles calculations using the VASP code were completed, and the calculated total energies per formula unit (f.u.) are included in Figures 3 and 4. These results are consistent with refined site occupancies from single crystal diffraction experiments. Among the tetragonal examples, Y prefers the M2 and M3 sites, with a slight energetic preference for the M3 position. In addition, Y seeks to maximize a heterometallic environment, rather than to include other Y atoms in its coordination sphere. On the other hand, among the orthorhombic cases, La seeks out the M1 site, showing preference for a distribution that maximizes near neighbor La−La distances. Although placing La at the M3 sites eliminates close contacts between La atoms, this site is too small for the larger La atom.

Although replacing La atoms by smaller Y atoms leads to the gradual structural transition in the $La_{5-x}Y_xSi_4$ system, the coloring problems in tetragonal La_4YSi_4 and orthorhombic LaY_4Si_4 can be explained by conventional geometrical factors.[14,15] We summarize the average M−M near neighbor distances in the $La_{5-x}Y_xSi_4$ phases characterized by single crystal diffraction in Table 4. Not only do these distances decrease according to the sequence M1-M, M2-M, and M3-M, but they become smaller with increasing Y content. Therefore, the smaller atom Y prefers to occupy M3 sites, then the M2 sites, whereas the larger atom La prefers the M1 sites, regardless of structure-type.

Structural Transition in $La_{5-x}Y_xSi_4$. According to the Zintl−Klemm formalism,[50] the formal charges for isolated Si atoms and Si_2 dimers are, respectively, −4 and −6 to satisfy their electronic configurations, assuming a single bond in each Si−Si dimer. The corresponding charge balanced formulas for tetragonal La_5Si_4- and orthorhombic Gd_5Si_4-type compounds are the same, that is, $[(M^{3+})_5(Si_2^{6-})_2](3e^-)$, which indicates three electrons assigned to the conduction band. Since replacing La by Y has no effect on the valence electron

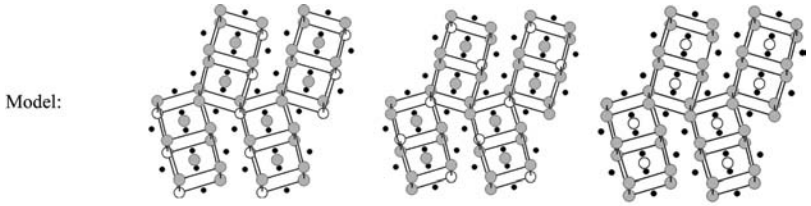

	(A)	(B)	(C)
Sites:	Y at 1/2 M1	Y at 1/2 M2	Y at M3
Space Group:	$P4_1$	$P4_1$	$P4_12_12$
E(meV/f.u.)	470.4	31.1	0
E(K/f.u.)	5459	361	0

Figure 3. Three models of tetragonal "La_4YSi_4". Gray dots are La atoms; black open circles are Y atoms; small black dots are Si atoms. The space group for each model is given. Total energies, relative to the lowest energy structure (**C**) and evaluated using VASP, are listed.

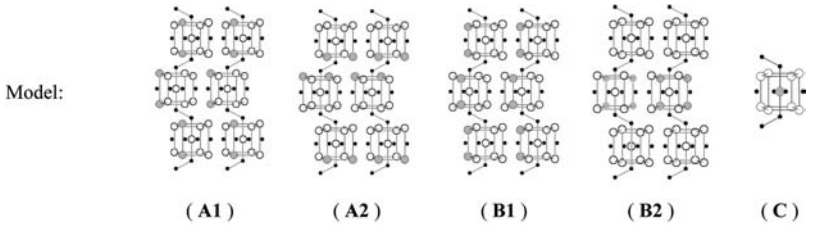

	(A1)	(A2)	(B1)	(B2)	(C)
Site:	La at 1/2 M1		La at 1/2 M2		La at M3
Space Group:	$Pnm2_1$	$P112_1/a$	$Pnm2_1$	$P2_1ma$	$Pnma$
E(meV/f.u.)	0	24	1009	1032	861
E(K/f.u.)	0	278	11700	12000	9990
La-La Dist.(Å)	4.517	3.885/3.994	3.746	3.746/3.892	-----

Figure 4. Five models of orthorhombic "LaY_4Si_4". Gray dots are La atoms; black open circles are Y atoms; small black dots are Si atoms. The space group for each model is given. Total energies, relative to the lowest energy structure (**A**) and evaluated using VASP, are listed.

Table 4. Average M-M Near Neighbor Distances (Å) in the $La_{5-x}Y_xSi_4$ Series

	average bond distance (Å)		
loaded composition	M1-M	M2-M	M3-M
La_5Si_4	4.104	4.046	3.673
La_4YSi_4	4.029	3.972	3.627
$La_2Y_3Si_4$	3.917	3.862	3.532
LaY_4Si_4	3.907	3.800	3.495
$La_{0.5}Y_{4.5}Si_4$	3.890	3.783	3.479
Y_5Si_4	3.884/3.890	3.786/3.805	3.469

count, the observed structural transitions are likely driven by the changing phase volume. Therefore, to investigate energy-volume relationships in $La_{5-x}Y_xSi_4$, VASP calculations were carried out on La_5Si_4 and Y_5Si_4 in the three different structure types: tetragonal (Pearson symbol *tP*36); orthorhombic (*oP*36); and monoclinic (*mP*36). To construct the models for these calculations, we used the experimental structures of La_5Si_4 (*tP*36), Gd_5Si_4 (*oP*36), and Y_5Si_4 (*mP*36), and simply varied the unit cell volume while keeping the structural shape intact. Figure 5 illustrates the three $E(V)$ curves for each compound; calculated values of relative total energies for each structure type are fit to the Murnaghan equation of state.[51] Table 5 summarizes the equilibrium unit cell volumes and relative total energies for each compound in the three structure types.

Table 5. Relative Eenergies[a] and Unit Cell Volumes[b] for La_5Si_4 and Y_5Si_4 Based on Fitting the VASP $E(V)$ Results with the Murnaghan Equation of State (EOS)[c]

		exp.	calc. (Murnaghan EOS Fit)	
compound	structure type	V^b	$V_{eq}{}^b$	E^a
La_5Si_4	*tP*36	250.3(1)	251.0	0.0
	*oP*36		249.0	165.4
	*mP*36		250.4	221.6
Y_5Si_4	*tP*36		212.7	99.9
	*oP*36		210.0	3.1
	*mP*36	208.3(1)	211.3	0.0

[a] In meV/f.u. [b] In Å^3/f.u. [c] As calculated for the three structural cases: tetragonal (*tP*36), orthorhombic (*oP*36), and monoclinic (*mP*36). The experimental unit cell volumes (in Å^3/f.u.) are included for the experimental structures.

The results in Figure 5 and Table 5 lead to the following inferences: (1) in agreement with experiment, La_5Si_4 prefers the tetragonal structure, Y_5Si_4 slightly prefers the monoclinic structure, but the orthorhombic Gd_5Si_4 is energetically competitive; (2) the ground state volume for La_5Si_4 is larger than for Y_5Si_4, in accordance with the relative atomic sizes of La and Y; (3) the equilibrium volumes for the three structure types tend to increase along the sequence orthorhombic-monoclinic-tetragonal for both cases; and (4) preference for the tetragonal structure increases at higher volumes (and, thus, lower

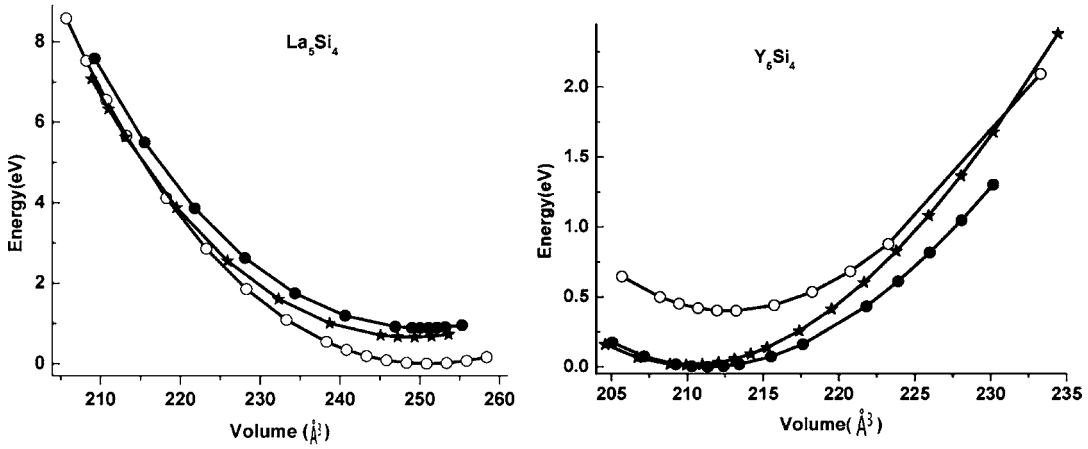

Figure 5. $E(V)$ curves of (left) La_5Si_4 and (right) Y_5Si_4 calculated using VASP for three distinct structure types: (i) tetragonal Zr_5Si_4-type (*tP*36; -○-); (ii) orthorhombic Gd_5Si_4-type (*oP*36; -*-); and (iii) monoclinic $Gd_5Si_2Ge_2$-type (*mP*36; -●-). The unit of volume is Å^3/f.u.

dx.doi.org/10.1021/ic201840q | Inorg. Chem. 2011, 50, 12714–12723

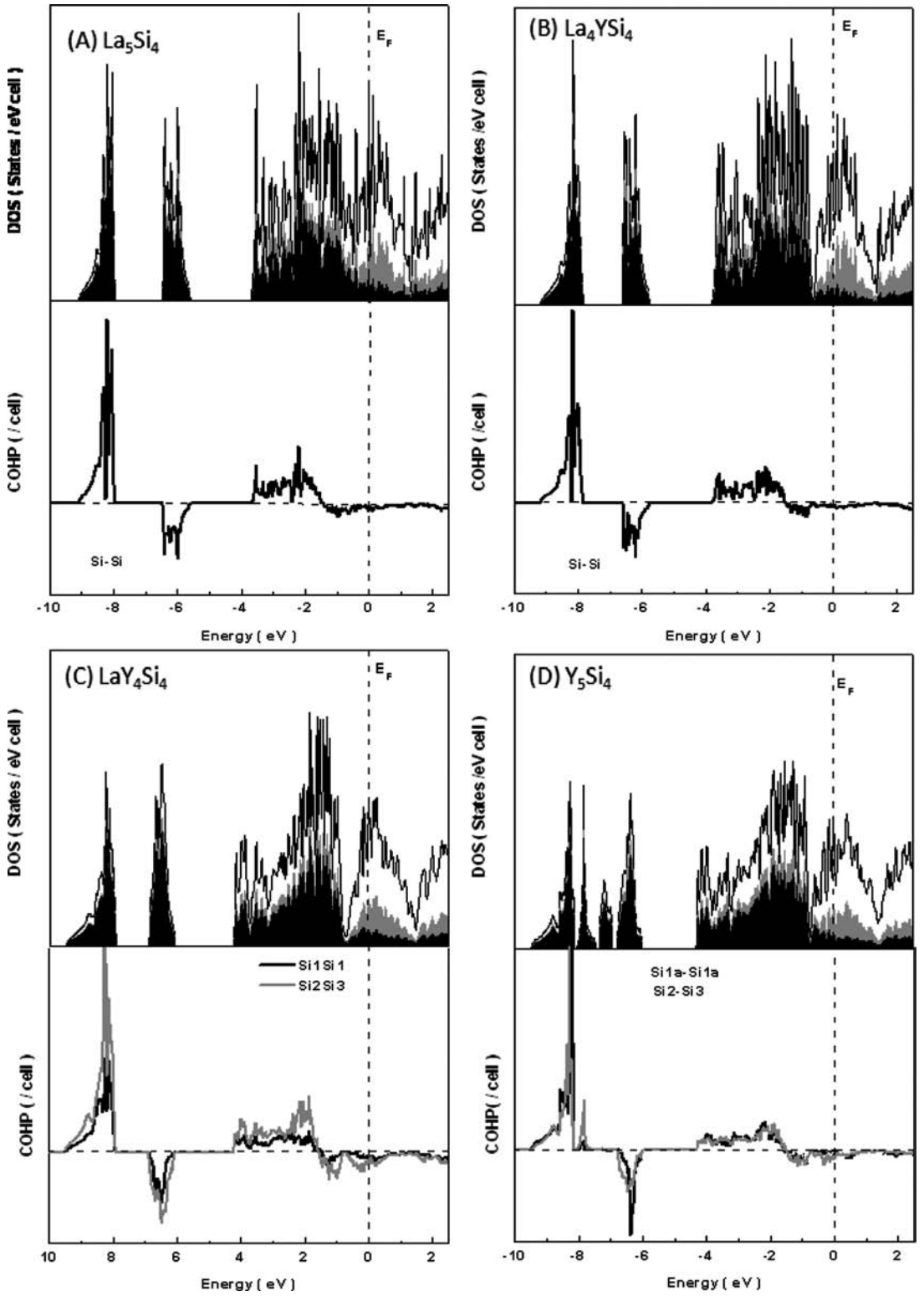

Figure 6. DOS and Si–Si COHP curves for (A) tetragonal La_5Si_4, (B) tetragonal La_4YSi_4, (C) orthorhombic LaY_4Si_4, and (D) monoclinic Y_5Si_4. Fermi levels are marked by dashed lines at 0 eV. In the DOS curves, Si contributions are emphasized in black; M3 site contributions are noted in gray.

pressures), whereas the orthorhombic and monoclinic structures are preferred at lower volumes (higher pressures). The fourth conclusion arises by examining the $E(V)$ curves for La_5Si_4 and Y_5Si_4 away from their equilibrium volumes. From the computational perspective, the agreement between experimental and computational equilibrium volumes is extraordinary, with the computed volumes slightly larger than experimental volumes, a result which can be attributed to the PBE pseudopotentials[52] used by VASP and has been observed in other reports also.[53,54] Further computational studies are currently underway to examine the complex interplay among structure type preference, chemical composition, and metal

dx.doi.org/10.1021/ic201840q | Inorg. Chem. 2011, 50, 12714–12723

atom distributions. Nonetheless, the structural differentiation in the $La_{5-x}Y_xSi_4$ series seems to be dominated by size factors that affect the packing of the building blocks, $(M3)M_8Si_6$ units (see Figure 1), rather than electronic factors, which can greatly influence the structures and atomic distributions among various Sm_5Ge_4-type and Gd_5Si_4-type structures.[55]

Electronic factors, however, cannot be ignored in this series. Monoclinic Y_5Si_4 has 1.5 Si_2 dimers and 1 Si monomer per formula unit, which creates the corresponding charge balanced formula $[(Y^{3+})_5(Si_2^{6})_{1.5}(Si^{4-})](2e^-)$ and indicates two electrons assigned to the conduction band. Thus, in Y_5Si_4, the numbers of dimers as well as valence electrons available for metal−metal bonding in the conduction band decrease after replacing La entirely by Y. Since the total number of valence electrons remains constant, these changes reflect redistribution of the valence electron density. As shown in Figure 5 and Table 5, the energy differences between the orthorhombic and the monoclinic structures are rather small, so it is, indeed, reasonable that some impurities, especially carbon, could stabilize one structure over the other.

Electronic Effects in $La_{5-x}Y_xSi_4$. To examine electronic effects in the $La_{5-x}Y_xSi_4$ series, electronic DOS and Si−Si COHP curves of tetragonal La_5Si_4 and La_4YSi_4 (model **C**, see Figure 3), orthorhombic LaY_4Si_4 (model **A1**, see Figure 4), and monoclinic Y_5Si_4 were calculated using the TB-LMTO-ASA code, analyzed, and illustrated in Figure 6. All total DOS curves share some similar features, the most noticeable of which are narrow bands, which are largely Si−Si σ_{3s} and σ_{3s}* orbitals, located 6.5−9.0 eV below the corresponding Fermi levels (E_F, 0 eV). In monoclinic Y_5Si_4, there are three distinct Si−Si "dimers," which have distances 2.494(6) Å (Si1a−Si1a), 2.573(2) Å (Si2−Si3), and 3.388(7) Å (Si1b−Si1b), the last of which is rather long to be considered a "covalently bonded" Si_2 dimer. The effect of this extension is the presence of two additional peaks lying between the Si−Si σ_{3s} and σ_{3s}* orbitals of the two shorter dimers. The conduction bands all begin about 4 eV below the Fermi levels. The lower, occupied portions are mostly derived from Si 3p orbitals, but Si's contribution drops significantly for states within about 0.5−0.7 eV below E_F. In the cases including Y, that is, tetragonal La_4YSi_4, orthorhombic LaY_4Si_4, and monoclinic Y_5Si_4, below E_F there are deep pseudogaps at the energies where this Si contribution changes abruptly. In the DOS curve for La_5Si_4, the pseudogap is less distinct, and the change in Si 3p contribution is more gradual. Interestingly, these pseudogaps in the DOS curves correspond to 28 valence electrons per RE_5Si_4 unit, which can be formally assigned to two 14-electron $(Si_2)^{6-}$ units. Among the occupied states in the DOS curves, the Si−Si COHP curves reveal weak antibonding orbitals, which would correspond to π* orbitals of these 14-electron dimers. However, the site symmetry of these Si−Si dimers is quite low, so complete decomposition of the DOS into the dimer orbitals does not occur. Above the pseudogaps, there are greater contributions from valence s and d orbitals of La or Y, with orbitals from the M3 sites participating greatest at the Fermi levels.

At present, there are no immediate clues from the electronic DOS or COHP curves of $La_{5-x}Y_xSi_4$ to suggest electronic factors driving the change in crystal structure along the series. Nonetheless, there are some subtle effects in the crystal structures, which affect the electronic structures that deserve attention. The most noticeable characteristic among the DOS curves, again, is the deep pseudogap in the occupied portion of the conduction band for the Y-containing examples. In all three of these cases, Y occupies the M3 site, which sits inside a distorted cube of metals and is surrounded by a distorted octahedron of Si atoms. This pseudogap in the DOS curves calculated by placing Y atoms in the other sites, M1 or M2 sites (see Figures 3 and 4) becomes less sharp, but remains noticeable. This result also emerges regardless of the computational method; similar DOS curves resulted from using VASP as well as TB-LMTO-ASA codes.

To obtain a preliminary assessment of the subtle differences between La and Y, bandwidths of specific regions of the electronic DOS curves of tetragonal La_5Si_4, tetragonal La_4YSi_4 (model 3, Figure 3), and orthorhombic LaY_4Si_4 (model A1, Figure 4) were evaluated at three different volumes; these results are listed in Table 6. For the cases of tetragonal La_5Si_4 and La_4YSi_4, both of which were calculated at different unit cell volumes, as the volume decreases, the bandwidths of all regions of the DOS curves increase, because the pairwise orbital overlaps increase. Evaluation of the Si−Si contribution to each region, as indicated by the integrated DOS (IDOS), also shows greater orbital mixing between Si−Si states and the surrounding rare-earth valence d orbitals as the volume decreases, an effect which leads to depletion of occupied orbitals assigned to Si for lower volumes. A comparison of the bandwidths and Si contributions to the Si−Si σ_{3s} and σ_{3s}* bands in La_5Si_4 and La_4YSi_4 at equal volumes reveals greater Y−Si and La−Si orbital mixing, especially in terms of their bandwidths, and less distinctly in terms of the integrated DOS. The Mulliken electronegativities[56] of Y (3.2 eV) and La (3.1 eV) suggest that the valence 4d and 5s orbitals of Y are slightly lower in energy than the 5d and 6s orbitals of La, which agrees with these subtle outcomes in the DOS analysis. In addition, we observe a slight increase to the Si−Si distance as Y content increases in the tetragonal $La_{5-x}Y_xSi_4$ samples, a result that can be interpreted as either weaker Si−Si interactions or stronger Y−Si over La−Si interactions with increasing Y content. Both changes in interactions seemingly occur, according to the DOS analysis.

Table 6. Bandwidths[a] and Si−Si Contributions[b] from Selected Regions of DOS Curves for Different Models of Tetragonal La_5Si_4 and La_4YSi_4 and Orthorhombic LaY_4Si_4[c]

compound (Å^3/f.u.)	Si−Si σ (eV)[d]	Si−Si σ* (eV)[d]	C.B. below E_F (eV)[d]	C.B. to 28e$^-$/f.u. (eV)[d]
La_5Si_4 (250.98)*	1.18 (1.39)	0.89 (1.26)	3.70 (4.10)	3.19 (3.87)
La_5Si_4 (238.58)	1.31 (1.36)	1.00 (1.26)	3.73 (4.11)	3.20 (3.88)
La_5Si_4 (213.22)	1.46 (1.35)	1.35 (1.19)	4.02 (3.93)	3.48 (3.36)
La_4YSi_4 (250.98)	1.23 (1.38)	0.75 (1.23)	3.72 (4.09)	3.10 (3.88)
La_4YSi_4 (238.58)*	1.38 (1.35)	0.85 (1.23)	3.81 (4.10)	3.15 (3.90)
LaY_4Si_4 (213.22)*	1.60 (1.34)	0.82 (1.25)	4.24 (4.44)	3.53 (4.22)

[a]In eV. [b]IDOS values, which equal # e$^-$, in parentheses. [c]Volumes per formula unit (f.u.) are given in parentheses under the compound heading. C.B. is conduction band; * in first column indicates observed volume. [d](Si_2 IDOS).

dx.doi.org/10.1021/ic201840q | Inorg. Chem. 2011, 50, 12714−12723

CONCLUSIONS

The $La_{5-x}Y_xSi_4$ series, x = 0, 1.0, 2.0, 3.0, 4.0, 4.5, and 5.0, crystallize in three different structures: (i) phases $x \leq 3.0$ exhibit the tetragonal Zr_5Si_4-type structure; (ii) phases x = 4.0 and 4.5 adopt the orthorhombic Gd_5Si_4-type structure; and (iii) the phase with x = 5.0 form the monoclinic $Gd_5Si_2Ge_2$-type structure. All of these different RE_5T_4-type structures have a common structural unit, $(M3)M_8Si_6$. The difference between these structures lies in how the $(M3)M_8Si_6$ units are interconnected and arranged in space. Single crystal X-ray diffraction indicates that Y atoms prefer to occupy the M3 sites, which have lowest volume increments; La atoms prefer the M1 sites, which have highest volume increments. These results from refinements are in line with first principles calculations on different models of La_4YSi_4 and LaY_4Si_4. The structural transition along the $La_{5-x}Y_xSi_4$ series can be attributed to size factors, whereas any electronic influences remain elusive. Nonetheless, the distribution of Y and La atoms among the various metal sites do influence the electronic DOS curves, and affect the characteristics of a pseudogap just below their corresponding Fermi levels.

ASSOCIATED CONTENT

Supporting Information

Single crystal refinement data in CIF format, interatomic distances and coordination polyhedral in $La_{5-x}Y_xSi_4$, atomic coordinates of La_5Si_4 and Y_5Si_4 used for the computational models in Figure 5, total DOS curves of different models of LaY_4Si_4 and La_4YSi_4 from LMTO and VASP calculations, and the DOS ratios vs energy for M/Si, M3/Si, and (M1+M2)/M3. This material is available free of charge via the Internet at http://pubs.acs.org.

AUTHOR INFORMATION

Corresponding Author

*E-mail: gmiller@iastate.edu.

ACKNOWLEDGMENTS

This work was supported by the U.S. Department of Energy, Office of Basic Energy Science, Division of Materials Sciences and Engineering. The research was performed at the Ames Laboratory. Ames Laboratory is operated for the U.S. Department of Energy by Iowa State University under Contract No. DE-AC02-07CH11358.

REFERENCES

(1) Smith, G. S.; Tharp, A. G.; Johnson, Q. *Nature* **1996**, *210*, 1148.
(2) Smith, G. S.; Johnson, Q.; Tharp, A. G. *Acta Crystallogr.* **1967**, *22*, 269.
(3) Smith, G. S.; Tharp, A. G.; Johnson, Q. *Acta Crystallogr.* **1967**, *22*, 940.
(4) Miller, G. J. *J. Chem. Soc. Rev.* **2006**, *35*, 799.
(5) Magen, C.; Morellon, L.; Algarabel, P. A.; Marquina, C.; Ibarra, M. R. *J. Phys.: Condens. Matter* **2003**, *15* (14), 2389−2397.
(6) Levin, E. M.; Pecharsky, V. K.; Gschneidner, K. A. *Phys. Rev. B* **2001**, *63*, 174110.
(7) Stankiewicz, J.; Morellon, L.; Algarabel, P. A.; Ibarra, M. R. *Phys. Rev. B* **2000**, *61* (19), 12651−12653.
(8) Levin, E. M.; Pecharsky, V. K.; Gschneidner, K. A.; Tomlinson, P. *J. Magn. Magn. Mater.* **2000**, *210* (1−3), 181−188.
(9) Morellon, L.; Blasco, J.; Algarabel, P. A.; Ibarra, M. R. *Phys. Rev. B* **2000**, *62* (2), 1022−1026.
(10) Levin, E. M.; Pecharsky, V. K.; Gschneidner, K. A. *Phys. Rev. B* **1999**, *60* (11), 7993−7997.
(11) Morellon, L.; Stankiewicz, J.; Garcia-Landa, B.; Algarabel, P. A.; Ibarra, M. R. *Appl. Phys. Lett.* **1998**, *73* (23), 3462−3464.
(12) Morellon, L.; Algarabel, P. A.; Ibarra, M. R.; Blasco, J.; Garcia-Landa, B.; Arnold, Z.; Albertini, F. *Phys. Rev. B* **1998**, *58* (22), 14721−14724.
(13) Pecharsky, V. K.; Gschneidner, K. A. *Phys. Rev. Lett.* **1997**, *78* (23), 4494−4497.
(14) Pecharsky, V. K.; Gschneidner, K. A. *Pure Appl. Chem.* **2007**, *79* (8), 1383−1402.
(15) Pecharsky, A. O.; Pecharsky, V. K.; Gschneidner, K. A. Jr. *J. Alloys Compd.* **2004**, *379*, 127.
(16) Pecharsky, A. O.; Gschneidner, K. A.; Pecharsky, V. K.; Schindler, C. E. *J. Alloys Compd.* **2002**, *338*, 126.
(17) Gschneidner, K. A. Jr.; Pecharsky, V. K.; Pecharsky, A. O.; Ivtchenko, V. V.; Levin, E. M. *J. Alloys Compd.* **2000**, *303*−*304*, 214.
(18) Yang, H. F.; Rao, G. H.; Liu, G. Y.; Ouyang, Z. W.; Liu, W. F.; Feng, X. M.; Chu, W. G.; Liang, J. K. *J. Alloys Compd.* **2003**, *361* (1−2), 113−117.
(19) Misra, S.; Miller, G. J. *J. Am. Chem. Soc.* **2008**, *130* (42), 13900−13911.
(20) Misra, S.; Poweleit, E. T.; Miller, G. J. *Z. Anorg. Allg. Chem.* **2009**, *635* (6−7), 889−897.
(21) Spichkin, Y. I.; Pecharsky, V. K.; Gschneidner, K. A. *J. Appl. Phys.* **2001**, *89* (3), 1738−1745.
(22) Ponweiser, N.; WarczoK, P.; Lengauer, C. L.; Richter, K. W. *Solid State Sci.* **2009**, *11*, 395−401.
(23) Rodewald, U. C.; Heying, B.; Johrendt, D.; Hoffmann, R. D.; Pottgen, R. *Z. Naturforsch. B* **2004**, *59* (2), 174−181.
(24) Guloy, A.; Corbett, J. D. *J. Solid State Chem.* **2005**, *178* (4), 1112−1124.
(25) Bulanova, M. V.; Zheltov, P. N.; Meleshevich, K. A.; Saltykov, P. A.; Effenberg, G.; Tedenac, J. C. *J. Alloys Compd.* **2001**, *329* (1−2), 214−223.
(26) Hunter, B. A.; Howard, C. J. *LHPM-Rietica*, 1.71; Australian Nuclear Science and Technology Organization: Menai, Australia, 2000.
(27) *SMART*, 5.625; Bruker AXS Inc.: Madison, WI, 2001.
(28) Hunter, B. A.; Howard, C. J. *SAINT+*, 6.22; Bruker AXS Inc.: Madison, WI, 2001.
(29) *SADABS*, 2.03; Bruker AXS Inc.: Madison, WI, 2001.
(30) *SHELXTL*, 6.10; Bruker AXS Inc.: Madison, WI, 2000.
(31) Kresse, G.; Furthmuller, J. *Comput. Mater. Sci.* **1996**, *6* (1), 15−50.
(32) Kresse, G.; Furthmuller, J. *Phys. Rev. B* **1996**, *54* (16), 11169−11186.
(33) Kresse, G.; Hafner, J. *Phys. Rev. B* **1993**, *47* (1), 558−561.
(34) Kresse, G.; Hafner, J. *Phys. Rev. B* **1994**, *49* (20), 14251−14269.
(35) Jepsen, O.; Andersen, O. K. *TB-LMTO*, 47; MPI-FKF: Stuttgart, Germany, 2000.
(36) Kresse, G.; Joubert, D. *Phys. Rev. B* **1999**, *59* (3), 1758−1775.
(37) Monkhorst, H. J.; Pack, J. D. *Phys. Rev. B* **1976**, *13* (12), 5188−5192.
(38) Dronskowski, R.; Blochl, P. E. *J. Phys. Chem.* **1993**, *97* (33), 8617−8624.
(39) Barth, U. V.; Hedin, L. *J. Phys. C: Solid State Phys.* **1972**, *5* (13), 1629.
(40) Koelling, D.; Harmon, B. N. *J. Phys. C* **1977**, *10*, 3017.
(41) Lambrecht, W. R. L.; Andersen, O. K. *Phys. Rev. B* **1986**, *34* (4), 2439−2449.
(42) Polotskaya, R. I.; Sidorko, V. R. *Powder Metall. Met. Ceram.* **1997**, *36*, 315−319.
(43) Shannon, R. D. *Acta Crystallogr.* **1976**, *A32*, 751.
(44) Hafner, J. *J. Phys. F: Met. Phys.* **1985**, 15.
(45) Koch, E.; Fischer, W. *Z. Kristallogr.* **1996**, *211*, 251−253.
(46) Pecharsky, V. K.; Gschneidner, K. A. *Adv. Mater.* **2001**, *13* (9), 683−686.
(47) Miller, G. J. *Eur. J. Inorg. Chem.* **1998**, *5*, 523.
(48) Mozharivskyj, Y.; Franzen, H. F. *J. Alloys Compd.* **2001**, *319* (1−2), 100−107.

(49) Mozharivskyj, Y.; Kaczorowski, D.; Franzen, H. F. *J. Solid State Chem.* **2000**, *155* (1), 259−272.
(50) Miller, G. J. In *Chemistry, Structure, and Bonding of Zintl Phases and Ions*; Wiley-VCH: New York, 1996; pp 1−59.
(51) Murnaghan, F. D. *Proc. N. A. S.* **1944**, *30*, 244−247.
(52) Perdew, J. P.; B., K.; Ernzerhof, M. *Phys. Rev. Lett.* **1996**, *77*, 3865.
(53) Stoffel, R. P.; Wessel, C.; Lumey, M. W.; Dronskowski, R. *Angew. Chem., Int. Ed.* **2010**, *49* (31), 5242−5266.
(54) Haas, P.; T., F.; Blaha, P.; Schwarz, K.; Laskowski, R. *Phys. Rev. B* **2009**, *80*, 195109.
(55) Wang, H.; Misra, S.; Wang, F.; Miller, G. J. *Inorg. Chem.* **2010**, *49* (10), 4586−4593.
(56) Pearson, R. G. *Inorg. Chem.* **1988**, *27*, 734.